One-dimensional dynamic model of a paper forming process

PAUL F. TURNBULL, NOEL C. PERKINS, WILLIAM W. SCHULTZ, AND PAUL D. BEUTHER

ABSTRACT

Fundamental conservation laws provide a one-dimensional, unsteady model of the wet end of a paper forming process. The authors approximate the stock as an inviscid fluid and the wire as an axially moving medium subjected to a fluid loading. Predictions of forming lengths are reasonable when compared to test data. Despite heavy damping, the model shows significant amplification of disturbances near resonant frequencies resulting in significant machine direction basis weight variations.

Application:

A one-dimensional model of a paper forming process on a single wire crescent former can describe both dynamic and steady state behavior of the forming process.

THIS STUDY FOCUSES ON THE mechanics of the wet forming region of a paper process. The motivation for the study was an understanding of the formation of tissue in a crescent forming machine. The crescent forming process involves a water and fiber fluid stock sprayed as a jet at a porous wire screen. The wire allows the water to pass through but traps the fibers. The wire forms a wide, continuous, and translating belt and wraps around a large roll called the form roll. This study only considers one-sided drainage. The forming region illustrated in **Fig. 1** extends from the point where the fluid jet impinges on the wire to the point where the fibrous mat touches the roll.

Previous theoretical models of paper forming focus on general measures of the forming process. They do not provide detailed or comprehensive descriptions of mat formation. An early theoretical study of the forming region by Miller *(1)* sought to estimate the total drainage rate through the mat and wire. A later study *(2)* made improvements in the drainage estimate specifically for a fourdrinier machine that passes a wire horizontally over a series of small rollers during the drainage process. Using an assumption of symmetry, Baines *(3)* examined the mechanics of a two-wire machine that permits water to pass through an inner wire and porous roll and an outer wire. The assumed symmetry in the forming region is inconsistent with the inclusion of centrifugal terms in the pressure equation. Turnbull *(4)* briefly described modifications of the model presented here for the two-wire machine. Until now, all models of the forming region assumed that the forming process was steady state. Direct observations of wire vibration and variations in mat thickness—variations in basis weight—indicate that the forming process is often unsteady, however. An example is the recent work by Perrault *(5)*.

The wire falls within a broader class of dynamical systems commonly called axially moving materials *(6)*. Examples of other axially moving materials include band saw blades, translating cables, belts, and tapes. Wickert and Mote *(7)* review recent developments in the vibration and stability of axially moving material systems. Wire vibration leads to dynamic contact between the wire and roll. This changes the length of the vibrating span and may affect the wire response *(8, 9)*. Our investigation also relates to studies of the response of web-like elements in a surrounding fluid *(10, 11)*. In previous studies, modeling of the fluid response on the web uses "added mass" coefficients. The original derivation of these came from the swimming of a slender fish approximated as an impermeable, flexible structure in an infinite fluid medium *(12)*. The present application demands an alternate approach for modeling the fluid and structure interaction because it violates the assumptions of structure impermeability and infinite fluid medium.

The next section describes the mathematical model used to predict the mechanics of a paper forming process. Then there is a detailed explanation of the numerical implementation followed by the resulting predictions. The conclusions drawn from the results highlight how the coupled fluid and wire dynamics influence product quality.

THE MODEL

Direct observations of wire vibration in the forming region and nonuniform mat thickness indicate that the forming process is often unsteady. Several excitation mechanisms may drive this time dependent response. Foremost among these are time-dependent jet velocity perturbations from the net delivery system coming from the pump, headbox, etc. Secondary excitation sources include fluid turbulence, roll eccentricity, periodic passage of wire splices, and mechanical perturbations originating from operations outside the forming region. Due to the slender geometry of the forming region, these seemingly small excitation

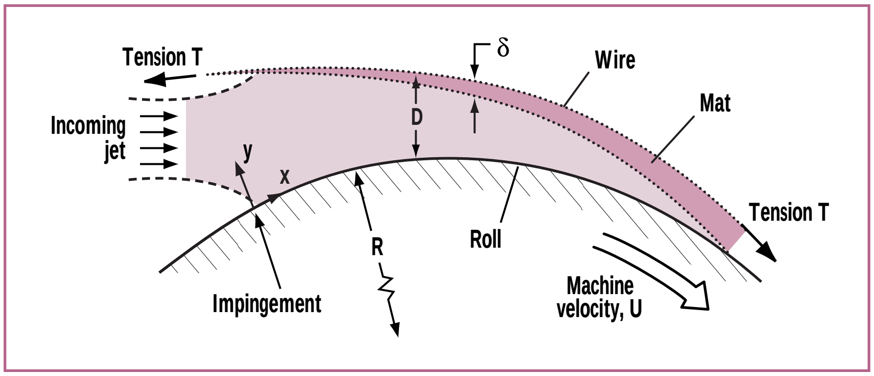

1. Schematic of the forming region

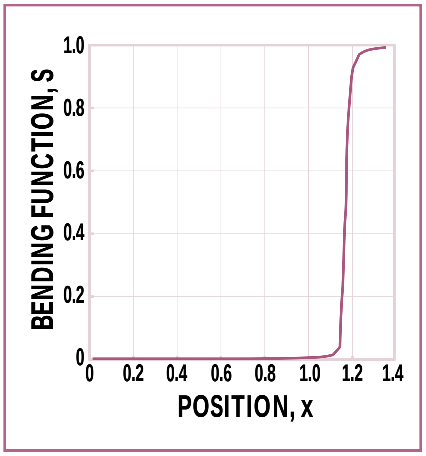

2. An example of the function s(x) used to blend the fluid-dominated and structure dominated subdomains

sources have the potential to generate large process impairing wire vibrations.

Figure 1 defines the problem of interest and the model coordinate system. The x and y coordinate system is curvilinear and locally Cartesian. The arc length along the roll defines x, and the position along the direction normal to the roll defines y. The origin of the coordinate system is at the fluid impingement point with the roll that is assumed stationary. We further assume no variation in the third direction—the cross direction (CD). $D(x, t)$ denotes the gap between the wire and the form roll. The mat thickness is $\delta(x, t)$, and the fluid velocity component in the x direction is $u(x, t)$. The form roll and the wire move with machine speed, U, and the wire has tension, T, in force per unit of width.

The fluid entering the domain has density, ρ; viscosity, μ; and a volumetric concentration of fibers, C_f. The Reynolds number, $\rho UD(x = 0)/\mu$, is large. This implies that the boundary layer along the roll will be thin, and viscous effects in the fluid will only occur in a small region near the end of the forming region. Assuming the fluid velocity is rectilinear, we can attempt to use an inviscid model. This leads to a one-dimensional model where x is the single independent spatial coordinate with the time variable, t.

The problem domain begins at a point shortly after the fluid impinges on the wire and roll. Here the fully three-dimensional flow of the entrance region has collapsed to a one-dimensional flow. This transition occurs almost immediately after wetting of both the wire and roll as shown in the section entitled "Steady-state response." The problem domain extends to a fixed position beyond the point where the mat is always in contact with the roll. The domain effectively splits into two subdomains:

- A fluid-dominated subdomain upstream from the contact point where the mat first touches the roll, $x <$
- A structure-dominated subdomain downstream from the contact point, $x >$.

The location of the contact point, , is unknown *a priori* but is found via the solution procedure. The primary difference between these two subdomains is the origin of the force supporting the wire. In the fluid-dominated subdomain, the force originates from the fluid pressure. In the structure-dominated subdomain, the contact of the fibers in the mat supplies the force. For the present formulation, we use a function that smoothly blends the governing equations for each subdomain together over a small region near the contact point, . In this small region, viscous forces are no longer negligible, making neither subdomain model strictly appropriate. Since mat formation is virtually complete before the transition between subdomains, however, the behavior of the model is insensitive to changes in the modeling of the downstream end.

Besides assuming inviscid flow, the principal modeling assumptions include the following:

1. The fluid impingement point is stationary.
2. There is no variation in the CD.
3. The wire vibrations are small, allowing assumptions that the wire tension, T, is constant and the wire curvature-displacement relation is linear.
4. The fluid velocity is rectilinear.
5. The void fraction of the mat, ε, is constant.
6. The mass of the wire per unit area including the mat and entrained water is constant in the wire equation.

Assumption 6 is the easiest to relax. For simplicity, however, we choose the average mass of the mat and wire to represent the mass for the entire length of the forming region. Relaxation of assumption 5 requires only a more elaborate model for the flow through the porous media. Relaxation of assumption 2 results in a two-dimensional extension of the present model. This is the subject of a subsequent study. Within the limits

Grid size	Time step
0.011	0.0017
0.0054	0.00045
0.0027	0.00014

I. Maximum stable time step vs. grid size

Parameter	Value	Units
Slice height, D_0	12.7	mm
Downstream height, D_L	0.168	mm
Upstream pressure, P_0	9000	Pa
Form roll radius	0.56	m
Machine speed	25.4	m/s
Wire tension	7881	N/m
Wire mass	1.0	kg/m^2
Headbox consistency, C_f	0.132	%
Void fraction, ε	0.9	
Jet/machine speed ratio	1.0	

II. Parameters defining the baseline system

of these assumptions, the governing equations derived below from the fundamental conservation laws are exact.

The following equation gives the conservation of water in one-dimension:

$$(1 - C_f)(D - \delta)_t + \varepsilon\delta^f = -[(1 - C_f)u(D - \delta) + \varepsilon U\delta]_x - v \quad (1)$$

where

C_f = the volumetric fiber concentration in the fluid
v = the apparent fluid velocity normal to the wire, the drainage velocity.

The subscripts, *t* and *x*, denote partial differentiation with respect to the variables. The terms on the left side account for the accumulation of water between the mat and the roll and in the mat. The difference between the change in the volume flow rate and the drainage velocity balance these terms.

Conservation of fiber mass provides the following equation:

$$C_m\delta_t + C_f(D - \delta)_t = -C_mU\delta_x - C_f[u(D - \delta)]_x \quad (2)$$

where

C_m = the volumetric fiber concentration in the mat (note that $C_m = 1 - \varepsilon$).

Here the left side of the equation represents the accumulation of fibers in the mat and in the fluid between the mat and roll. The accumulation is due to the change in the *x* direction of fibers being convected downstream in the mat and the fluid, respectively. One can simplify this expression for conservation of fibers to the following:

$$\delta_t + U\delta_x = -(C_f/C_m)\{(D - \delta)_t + [u(D - \delta)]_x\} \quad (3)$$

Neglecting fluid viscosity except in the mat, conservation of momentum yields the unsteady Euler equation:

$$u_t = uu_x = -(1/\rho)p_x \quad (4)$$

The Euler equation states that the pressure gradient determines the change of the fluid momentum along the machine direction (MD). The following equation governs the transverse response of the wire:

$$D_{tt} + 2UD_{xt} - U^2D_{xx} - U^2/R = (T/m)(D_{xx} - 1/R + p/T) \quad (5)$$

where

m (approximated as a constant)= the mass of the wire, the mat, and the entrained water per unit area
R = the form roll radius as shown in Fig. 1.

The terms on the left side of the equation represent the absolute acceleration of a wire element including the convective acceleration components due to wire translation around the form roll *(6)*. The term, *(T/m)* (1/*R*), on the right side of the equation results from the curvature of the coordinate system. The quantity *p* on the right side of Eq. 5 represents the force per unit that the fluid or mat exerts on the wire area. In the fluid dominated subdomain, $x <$, p is therefore the fluid pressure determined by the resistance of the flow through the mat using the following empirical relation:

$$p = a(\delta + \delta_w)v + b(\delta + \delta_w)v^2 \quad (6)$$

where

a = μk
b = $C_e\rho/(\kappa)^{1/2}$
κ = the permeability of the mat and wire determined by the fiber diameter and void fraction *(13)* of Eq. 1
μ = the viscosity of water
ρ = the density of water
C_e = the Ergun coefficient adjusted to fit experimental data as described in "Steady-state response"
δ_w = the resistance to flow through the wire expressed as an equivalent mat thickness.

In this study, δ_w is 10^{-5} m for 20-μ fibers with a void fraction of 90%, a = 2153 kg/m^3 · s. The term proportional to v^2 accounts for the inertial effects present in a thin porous media. In the limit of vanishing *b*, this expression becomes a one-dimensional integrated form of Darcy's law for flow through porous media. Note that the pressure, *p*, provides the coupling between the fluid and the wire. Since the pressure is proportional to *v* and v^2 that in turn relate

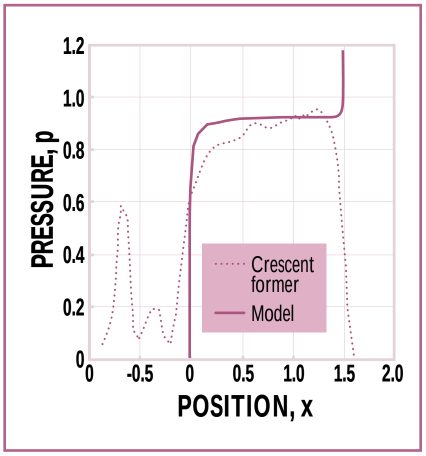

3. *The pressure profile as measured on a crescent former and as calculated by the model for the baseline system*

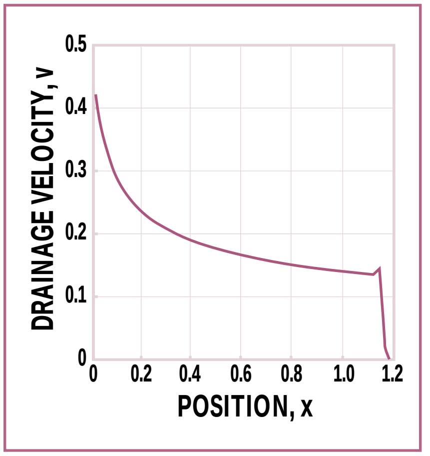

4. *The steady state drainage velocity, v, as a function of x for the baseline system*

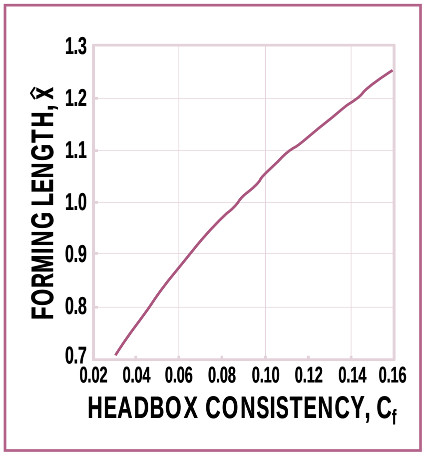

5. *The steady state forming length, , scaled by R as a function of the headbox consistency, C_f*

to D_t in Eq. 1, one may interpret the pressure as a nonlinear damping mechanism for wire vibration. The section entitled "Unsteady response" discusses this.

The translating wire supported by a compressible mat modeled as an elastic foundation describes the structure-dominated subdomain. Bhat *(14)*, Perkins *(15)*, and Tan *(16)* describe previous analyses of translating elements on elastic foundations. In this subdomain, Eq. 6 again governs the wire response where p is now the force per unit area created by an elastic foundation as follows:

$$p = k(F - D) \qquad (7)$$

where

k = an effective mat stiffness per unit area

F = a constant representing the free height of a theoretical distributed spring that balances the tension in the wire.

The constants, k and F, are such that the spring force, p, balances the tension, T, at the downstream boundary and the spring remains in compression for the full length of the structural domain. At steady state, p approaches T/R as D approaches δ. Computed results are insensitive to changes in k and F and in the modeling of the boundary between the fluid dominated and structure dominated subdomains. This insensitivity is due to the dominance of the fluid subdomain and the bias in the flow of energy downstream in the MD. Changes at this downstream boundary therefore exert little influence on the forming process occurring upstream.

One can make the above dependent variables dimensionless by employing the length scale defined by the form roll radius, R; the time scale, R/U; and a pressure scale, T/R. Equations 3–5 define a system of three partial differential equations that are fourth-order in time and fifth-order in space. The dimensionless equations are as follows:

$$\delta_t + \delta_x = -(C_f/C_m)\{(D-\delta)_t + [u(D-\delta)]_x\} \qquad (8)$$

$$U_t = -(T/\rho R U^2)p_x - uu_x \qquad (9)$$

$$D_{tt} + 2D_{xt} + D_{xx} - 1 = (T/mU^2)(D_{xx} - 1 + p) \qquad (10)$$

Completing the system of equations involves solving for v in Eq. 1. This results in the following:

$$v = -(1 - C_f)\{(D-\delta)_t + [u(D-\delta)]_x\} + \varepsilon(\delta_t + \delta_x) \qquad (11)$$

Substituting this result in Eq. 6 gives the following:

$$p = (R^2U/T(\delta + \delta_w)(av + bUv^2) \qquad (12)$$

The following equations provide the associated boundary conditions:

$$D(0, t) = D_0 \qquad (13a)$$

$$D(L, t) = D_L \qquad (13b)$$

$$\delta(0, t) = 0 \qquad (13c)$$

$$u(0, t) = U_0 \qquad (13d)$$

$$p(0, t) = P_0 \qquad (13e)$$

These boundary conditions may be time dependent to allow for possible excitation mechanisms including jet velocity fluctuations and roll eccentricity. Motion may also follow from initial conditions of the following forms:

$$D(x, 0) = f(x) \qquad (14a)$$

$$D_t(x, 0) = g(x) \qquad (14b)$$

$$\delta(x, 0) = q(x) \qquad (14c)$$

$$u(x, 0) = r(x) \qquad (14d)$$

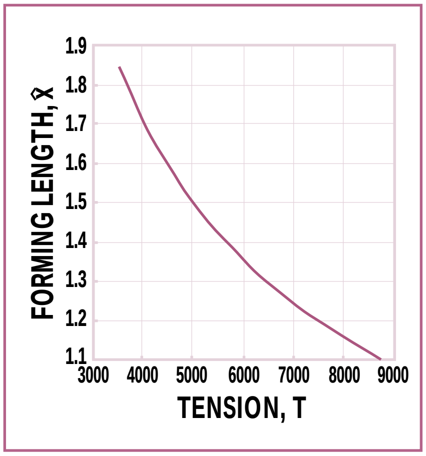

6. The steady state forming length, , scaled by R as a function of the wire tension, T, expressed in dimensional units of N/m

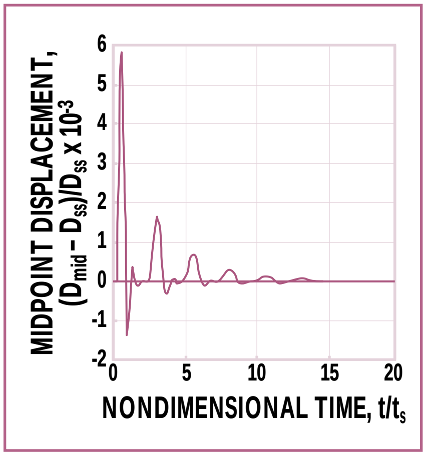

7. Transient wire response represented by the motion of the midpoint, x = L/2, of the wire normalized by the steady state displacement of the wire at the midpoint

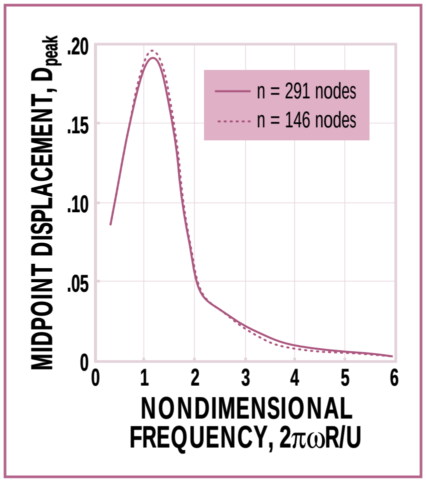

8. Frequency response of the wire at the midpoint, x = L/2

The above initial conditions also determine the initial drainage velocity, $v(x, 0)$, and the initial pressure profile, $p(x, 0)$, using Eqs. 11 and 12.

NUMERICAL ANALYSIS

This model couples a parabolic fluid advection equation (Eq. 9), a hyperbolic wave propagation equation (Eq. 10), and the equations governing the conservation of mass of an incompressible fluid and fiber stock (Eqs. 8 and 12). Taken separately, these different types of equations require qualitatively different solution strategies. There are also complexities due to the two subdomains needed to model the unknown location of the contact point. The numerical strategy must overcome a unique set of difficulties.

We solve the fluid advection equation (Eq. 9) using an upwind technique employing explicit, Adams-Bashforth time integration *(17)*. This method preserves the bias in the flow of information in the downstream direction and provides a method that is conditionally stable for sufficiently small time steps. The mat evolution equation (Eq. 8) and fluid conservation equation governing the pressure (Eq. 12) have less bias in the flow of information. Central-difference in space and Adams-Bashforth explicit time integration were conditionally stable. The fluid velocity and mat thickness are advected downstream in the structural subdomain using a first-order upwind method.

The wave equation (Eq. 10) governing the vibration of the wire is also discretized using central-difference approximations and integrated in time using a Crank-Nicolsen implicit method. Normally this scheme is unconditionally stable for arbitrary time steps. Due to the interaction with the fluid, however, the discretized version of Eq. 10 loses its unconditional stability. The scheme is conditionally stable for sufficiently small time steps. For example, **Table I** shows the maximum stable nondimensional time steps for three different nondimensional grid sizes.

The location of the contact point and therefore the length of the forming region are unknown and must be found as part of the solution of the system of equations. To accomplish this, the computational domain is split into two subdomains previously described. The two subdomains blend into a single continuous computational domain using a function, s, defined as follows:

$$s = 1/2\{\tanh [(c_1\delta/D) - c_2] + 1\} \quad (15)$$

where

$$0 < s < 1.$$

The equations governing the fluid-dominated subdomain are multiplied by $(1 - s)$, and those governing the structure-dominated subdomain are multiplied by s. One then adds these product equations. The constants, c_1 and c_2, are such that $s << 1$ over most of the forming region and then smoothly approaches $s \rightarrow 1$ when $\delta/D > 1$. **Figure 2** shows a typical shape of the blending function for $c_1 = 6$ and $c_2 = 3$.

It is possible to adjust the values chosen for the boundary conditions to simulate specific papermaking machines. The initial gap between the wire and roll, D_0, is equal to the height of the jet. The downstream boundary condition, D_L, is set to the theoretical steady state mat thickness based on global fiber conservation using the following:

$$D_L = C_f U_0 D_0 / c_m U \quad (16)$$

The jet velocity, U_0, is usually equal to the machine speed. One can set it lower or higher, however, to examine the effects of a velocity differential between the fluid and the wire. Such a velocity differential is typically desirable due to its influence on

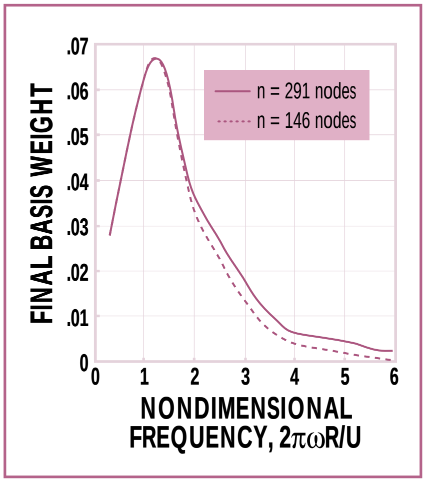

9. Frequency response of the basis weight of the mat leaving the forming region at x = L

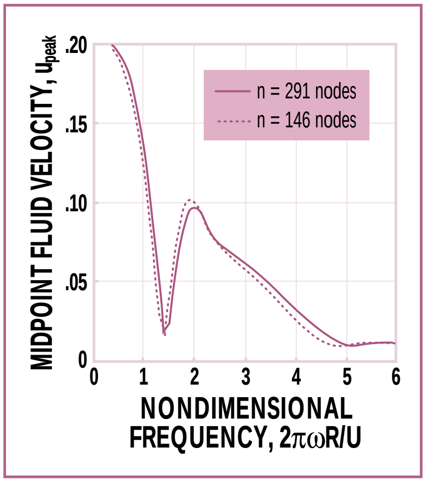

10. The frequency response of the fluid velocity, $u_{peak}(x = L/2) = (u_{max} - u_{ss})/u_{ss}$ for a jet velocity disturbance amplitude of 2% of the steady-state jet velocity for two values of n

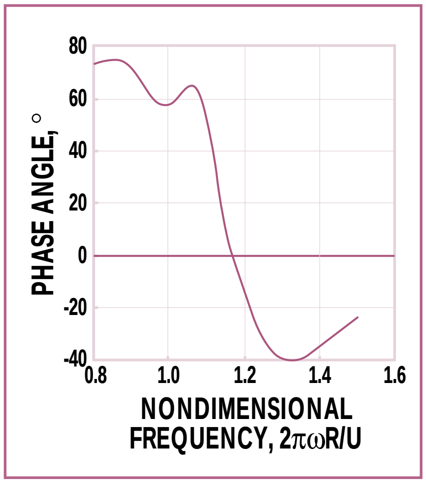

11. The phase difference between peaks in the wire displacement, D, and the fluid velocity, u

fiber orientation and the resulting influence on mat tensile strength.

It is not as easy to determine the pressure at the beginning of the one-dimensional region, P_0, however, due to higher dimensional entrance effects, i.e., transition from free jet to a confined fluid layer. The pressure after these entrance effects is unknown *a priori*. It is not possible to use the pressure measured at the roll to determine the pressure at the wire at the jet impingement. Instead, one chooses the pressure, P_0, to avoid substantial oscillations of the pressure profile. Iterating on P_0 until the quantity, $\delta^2 P(0, t) / \delta x^2 = 0$, accomplishes this. The method starts with the initial guess for the upstream pressure as $P_0 = T / 2R$, and a simulation is run to steady state. If $\delta^2 P(0, t)/\delta x^2 < 0$ at steady state, the value for P_0 is too small. Similarly, P_0 is too large if this second derivative is positive. The upstream pressure is subsequently adjusted to obtain a smooth pressure profile. Then P_0 is held constant during the subsequent simulations of unsteady response.

NUMERICAL RESULTS

We examined the above numerical method to examine both the steady-state and unsteady response of a paper forming process. Consider first the simpler steady-state case.

Steady-state response

We propose a baseline system for study as defined by the parameters shown in **Table II**. Unless otherwise noted, all computed results that follow pertain to this baseline system. The nondimensional mesh size chosen for almost all the steady-state computations to follow is 0.011. Since increasing the number of nodes does not appreciably alter the steady-state results, we conclude that the following results are well converged.

Without excitation, we expect a stable system to settle to a stable steady state following any perturbation, e.g., initial conditions. Determining the steady-state solution for a particular set of system parameters makes it possible to calibrate the adjustable parameter, b, by adjusting the Ergun coefficient, C_e, in the fluid resistance relation. This is accomplished by comparing computed results for the forming length to that measured on a forming machine operating with the same set of system parameters and adjusting b such that the forming lengths match. Alternatively, one may adjust all three parameters in the fluid resistance relation of Eq. 12, δ_w, a, and b, to produce a better fit of the forming length for broader operating conditions.

Major capabilities of the steady state model include the ability to predict the forming region geometry, the drainage profile, and the pressure profile. **Figure 3** shows an example of the predicted steady-state pressure profile with experimental measurements. In this figure, pressure, p, is scaled by T/R and position, x, is scaled by R. This type of comparison is used to calibrate the resistance parameter, b, in Eq. 12. From the comparison in Fig. 3, the adjustable parameter, b, was selected by setting $C_e = 14$ to match this test data. All subsequent results use this value.

Examination of the test data reveals an initial pressure spike occurring at the impingement of the fluid on the roll followed by a region of low pressure. At $x = -0.2$, both the wire and roll become wetted and the pressure rises monotonically. After a short entrance region, $-0.2 < x < 0$, the fluid mechanics have collapsed from the fully three-dimensional flow of the jet to the one-dimensional flow of the trapped fluid layer. From this point defined as $x = 0$, the assumptions of the model are valid

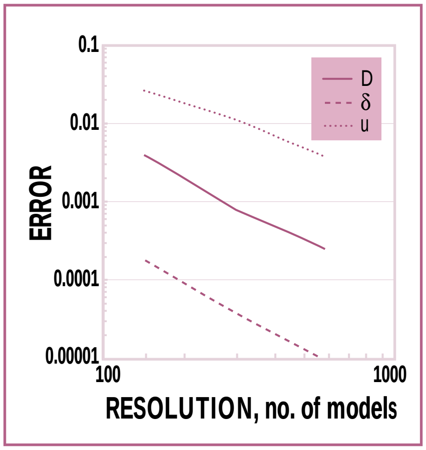

12. Quadratic spatial convergence of the three primary variables

and the computational domain begins. Note that the predicted pressure is nearly T/R for most of the fluid-dominated domain. This produces a wire geometry with very little curvature relative to the roll. The gap, D, between the wire and the roll therefore decreases almost linearly with the arc length coordinate, x. **Figure 4** shows that this nearly linear geometry occurs despite very nonuniform drainage velocity, v. In the figure, drainage velocity, v, is scaled by U, and position, x, is scaled by R. The final mat thickness was 1% less than the theoretical value given by global conservation of fibers from Eq. 16.

The model can predict the steady state geometry of the forming region for a range of parameters near those used to calibrate the parameter, b. For example, **Fig. 5** shows the variation in forming length with respect to the fiber concentration in the stock, C_f, the headbox consistency. **Figure 6** similarly shows the variation in forming length vs. tension. Both show smooth monotonic behavior over the range of parameters modeled. As expected, the forming length increases with increasing headbox consistency and decreases with increasing tension.

Unsteady response

The time-dependent model computes the system response under free and forced conditions. For free response, the system is perturbed by selected initial conditions, and the ensuing transient response is computed. For forced response, the system is perturbed by unsteady upstream boundary conditions. In all computations to follow, the response of selected quantities—wire displacement and fluid velocity—are sampled at the midpoint of the fluid dominated subdomain—a single node value—unless otherwise noted.

Consider first the free response of the wire as measured by the midpoint displacement, D_{mid}, above the roll as **Fig. 7** shows. Time is made dimensionless using the time scale, $t_s = R/U$. This response is normalized by the steady state displacement, D_{ss}, at the midpoint. The system is started from steady-state and given an initial transverse velocity with a maximum amplitude, $D_t = 0.01$, at the midpoint of the fluid-dominated subdomain and a half sine wave shape in x. From Fig. 7, it is apparent that there is a short period of transient response followed by a rapid relaxation to steady state. This short transient is evidence of the substantial damping inherent in the momentum equation for the wire. This damping is due to the energy lost as the fluid is forced through the porous media through the resistance relation for the flow through the mat and wire in Eq. 12. From the oscillations evident in the free response, it is also possible to estimate the natural frequency of the fundamental mode of the system. This has a period of approximately one time unit (nondimensional). Such oscillations lead to disturbances with a wavelength of approximately one roll radius.

Next consider the forced response of the system to a small harmonic variation in the inlet jet velocity given by $u(0, t) = u_0(1 + A \cos \omega t)$. Here u_0 is the steady component of the jet velocity—set equal to 1 in this example (equal to the wire velocity)—and A and ω are the amplitude and frequency of the dynamic component of the jet velocity. In this calculation, the forcing is held constant at $A = 0.01$ while the excitation frequency, ω, varies over the range $0 < \omega < 6$. For each value of ω, the system is integrated until it reaches a steady-state oscillation. The frequency response results of **Figs. 8–10**, respectively, report the amplitude of the variation in D,δ and u. In contrast to the steady-state computations, the grid resolution modestly influences the magnitude of the results. Results are shown for two grid sizes, $\Delta x = 0.011$ and $\Delta = 0.0054$, illustrating the small difference in response amplitude with increasing grid refinement. Temporal convergency is assured by selecting a time step an order of magnitude smaller than the time step required for stability at the spatial resolutions indicated.

Figure 8 shows the normalized peak midpoint displacement of the wire, D_{peak}, as a function of the excitation frequency. In the figure, the peak-to-peak amplitude of the stable limit cycle [$D_{peak} = (D_{max} - D_{ss})/D_{ss}$] is shown as a function of frequency for a jet velocity disturbance amplitude of 2% of the steady-state jet velocity for two values of n. The frequency response of the wire shows a single broad peak indicative of a single degree of freedom, heavily damped system. Although the wire has infinite degrees of freedom, damping suppresses the response of the higher frequency modes. The absence of higher order peaks in the wire frequency response of Fig. 8 shows this. The resonant behavior of the wire has a pronounced influence on the basis weight of the final product—computed from the mat thickness at the end of the forming region, $\delta(L, t)$— as Fig. 9 shows. In the figure, the peak to peak amplitude of the stable limit cycle [$\delta_{peak} = (\delta_{max} - \delta_{ss}) \delta_{ss}$] is shown as a function of frequency for a jet velocity disturbance amplitude of 2% of the steady state jet velocity for two values of n. Similar to the wire response, there is substantial disturbance amplification

KEYWORDS
Crescent formers, equations, flow, fluid flow, formation, forming, models, paper making, sheet formers, sheet forming, wet ends.

evident in the response of the basis weight. In addition, the disturbance wavelength is again approximately one roll radius. The frequency response of the peak fluid velocity, however, has a local minimum—antiresonance—near the frequency corresponding to the peak wire response that Fig. 10 shows. Examination of the phase relationship between the response of the wire and the fluid velocity explains this as detailed below.

Figure 11 shows the phase relationship between the wire and fluid responses near the local minimum in the peak fluid velocity. The phase was computed by comparing the time when the peak in the fluid velocity occurs vs. the time when the peak displacement of the wire occurs. Note that the drop in the peak fluid velocity occurs when the fluid response is in phase with the wire response. This is consistent with conservation of mass. If the displacement of the wire is increasing as the fluid velocity is increasing, there will be a greater volume for the fluid to occupy. This reduces the tendency of the fluid to accelerate.

As further support to the discussion on model convergency above, we provide an estimate of the rate of spatial convergency by employing Richardson extrapolation to estimate the exact values of the peak to peak variation in the three primary variables D, δ, and u, at a forcing frequency of $\omega = 1$. These estimated values of the primary variables determine the error at three grid sizes, $\Delta x = 0.011$ corresponding to $n = 146$ nodes, $\Delta x = 0.0054$ corresponding to $n = 291$ nodes, and $\Delta x = 0027$ corresponding to $n = 581$ nodes. **Figure 12** shows the results. The linear relationship between error and the number of nodes on the log-log plot illustrates quadratic convergence with n as expected for the finite difference algorithms used in the model.

CONCLUSIONS

We derived a one-dimensional model of a paper forming process on a single wire crescent former from fundamental conservation laws. The model can describe dynamic and steady state behavior of the forming process. Examination of predicted steady state geometry shows that the model gives the pressure profile, drainage velocity, and forming length with reasonable accuracy compared to test data. After calibrating the parameter, b, of Eq. 12, one can predict the steady state resulting from modest changes in the key process parameters such as tension, machine speed, headbox consistency, and the permeability characteristics of the mat and wire. The steady-state results therefore help to understand how these process parameters control the forming process without disturbances.

The free response of the model to an initial disturbance illustrates a large damping mechanism caused by the flow through the mat and wire. Computed frequency responses demonstrate that only the first system mode is excited and that higher modes of vibration are suppressed. The system effectively behaves therefore as if it were a single degree of freedom system. Despite the heavy damping, however, the model shows significant amplification of disturbances near resonant frequencies. The model predicts that 2% disturbances in jet velocity may result in nearly 7% variation in the basis weight due to the aforementioned resonance of the fundamental mode. In addition, the resulting wavelengths of these basis weight fluctuations are approximately the roll radii. An experimental study by Perrault *(5)* shows large amplifications of MD basis weight variations at particular frequencies. It is not possible to make direct comparisons to the analysis because of inadequate descriptions of the process parameters.

Our latest work relaxes two assumptions made herein by including the effects of viscosity and variations in the CD. The preliminary results indicate that the system solution remains remarkably similar to the one-dimensional inviscid model described here except in a very small region near the nip. The addition of viscosity appears to allow integration within a purely fluid computational domain nearly all the way to the nip without the requirement of a structure dominated model nor a blending function. **TJ**

Turnbull was a graduate research assistant now at Ford Motor Co., Perkins is associate professor, and Schultz is associate professor, at University of Michigan, Ann Arbor, MI 48109; and Beuther is associate research fellow, Kimberly-Clark Corp., 2300 Winchester Rd., Neenah, WI 54956.

The authors thank E-June Chen at University of Michigan and Jay Shands at Beloit Corp. for useful discussions on this work. They also acknowledge the Kimberly-Clark Corp. and the TAPPI Foundation for partial support of this study.

Received for review Dec. 22, 1995.

Accepted July 9, 1996.

LITERATURE CITED

1. Miller, G. F., *Proc. Royal Soc. London* 242: 1(1957).
2. Schoeffler, J. D., and Sullivan, P. R., *Tappi*49(6): 248(1966).
3. Baines, W. D., *Flow in the Formation Region of a Two-Wire Machine*, PAPRICAN, Montreal, 1970, pp. 1-29.
4. Turnbull, P. F.,*Analysis of a Paper Forming Process*, Ph.D. thesis. Univ. of Michigan, Ann Arbor, MI, 1995.
5. Perrault, J., *Tappi J.* 67(7): 62(1984).
6. Mote, C. D. Jr., *Shock and Vib. Digest* 4(4): 2(1972).
7. Wickert, J. A. and Mote, C. D. Jr., *Shock and Vib. Digest* 20(5): 3(1988).
8. Yue, M. G., *ASME 6th Int. Power Transmission and Gearing Conference* 43(1): 311(1992).
9. Turnbull, P. F., Perkins, N. C., and Schultz, W. W., *J. Vib. and Control* 1(4):459(1995).
10. Pramila, A., *J. Sound and Vib.* 113(1): 198(1987).
11. Chang, Y. B. and Moretti, P. M., *TAPPI 1990 Engineering Conference Proceedings*, TAPPI PRESS, Atlanta, p. 175.
12. Lighthill, M. J., *J. Fluid Mech.* 9(2): 305(1960).
13. Kaviany, M., *Principles of Heat Transfer in Porous Media*, Springer- Verlag, New York, 1991, pp. 62–64.
14. Bhat, R. B., Xistris, G. D., and Sankar, T. S., *ASME J. Mech. Design* 104(1): 143(1982).
15. Perkins, N. C., *ASME J. Vib. and Acoust.* 112(1): 2(1990).
16. Tan, C. A. and Zhang, J., *ASME J. Vib. and Acoust.* 116(3): 318(1994).
17. Peyret, R. and Taylor, T. D., *Computational Methods for Fluid Flow*, Springer-Verlag, New York, 1990, pp. 3–77.